Available online at www.sciencedirect.com
SCIENCE DIRECT®
Thin Solid Films 436 (2003) 292–297
thin solid films
www.elsevier.com/locate/tsf

Image force effects on trapezoidal barrier parameters in metal–insulator–metal tunnel junctions

X.C. Ma[a,*], Q.Q. Shu[a], S. Meng[b], W.G. Ma[b]

[a]*Department of Materials Science and Technology, School of Science, Shenzhen University, Shenzhen 518060, PR China*
[b]*Department of Modern Physics, University of Science and Technology of China, Hefei 230026, PR China*

Received 4 June 2002; received in revised form 26 February 2003; accepted 26 March 2003

Abstract

A one-dimensional trapezoidal barrier potential $U_0(x)$ *with* and *without* the image potential $U_i(x)$ was used to model three tunnel junctions: Al–Al_2O_3–Au (–Ag, –Cu) and calculate the junction I–V curves. As the effective trapezoidal barrier parameters are determined by fitting the calculated I–V curves to the experimental ones, it is found that if the I–V curves are calculated based on the barrier potential $U_0(x)+U_i(x)$, the parameters of the actual barrier $U_0(x)-U_i(x)$ are obtained. Thus, the parameters of the actual trapezoidal barrier $U_0(x)+U_i(x)$ can be obtained by extrapolating. The results show that the area of the actual $U_0(x)+U_i(x)$ is smaller than that of the $U_0(x)$ and for the Au-, Ag- and Cu-junction the area reduction is -6.9, -5.4 and -4.2%, respectively. The variation of the barrier area reduction with the electrodes can be ascribed to the diffusion and oxidation reaction in the region of the junction interfaces, which results in smeared and indistinct interfaces and an increase in the actual distance between the metal mirrors of the two electrodes.

Keywords: Tunneling; Interfaces; Image force; Trapezoidal barrier parameters

1. Introduction

The study of the image force effect on electron tunneling has proceeded since the tunneling probabilities through a metal surface barrier potential in the WKB approximation were calculated in 1928 [1–7]. It was found that the effect of the image force is to round off the corner of the surface barrier potential, as shown in Fig. 1, and that under the action of an electrical field the tunneling probabilities with the image force are approximately three orders as great as without the image force [1–3]. Later, for the biased metal–insulator–metal (MIM) tunnel junctions, the interaction of the tunneling electron in the trapezoidal barrier region with the two image charges located in the two metal electrodes, respectively, was treated carefully by Simmons [4]. His results show that the effect of the image force is to round the edges of the barrier and to slightly lower the average barrier height, and thus to somewhat increase the overall tunneling probability. Hence, in general, for simplicity the image force correction has been omitted. However, as all the barrier parameters are to be determined, the image force correction will become apparent and important because the image force modifies the barrier shape [5]. Recently, a numerical solution to the Schrödinger equation shows that the barrier lowering induced by the image potential affects the tunneling current largely in ultra-thin MOS structures [7]. Now, as the research interests in the ferromagnetic MIM tunnel junctions with giant magnetoresistance has been increasing rapidly, the determination of the barrier parameters by fitting the I–V curves has become a routine method to characterize the junctions [8,9]. In this paper, for three types of the junctions with Au, Ag and Cu top electrode, three groups of the barrier parameters with and without the image force were determined by fitting the calculated I–V curves to the experimental ones at 77 K, respectively, and the correlation between the metal electrodes and the barrier areas with inclusion of the image potential was discussed.

*Corresponding author. Tel.: +86-755-6538236; fax: +86-755-6534023.
E-mail address: maxiaocui@163.net (X.C. Ma).

0040-6090/03/$ - see front matter © 2003 Elsevier Science B.V. All rights reserved.
doi:10.1016/S0040-6090(03)00591-1

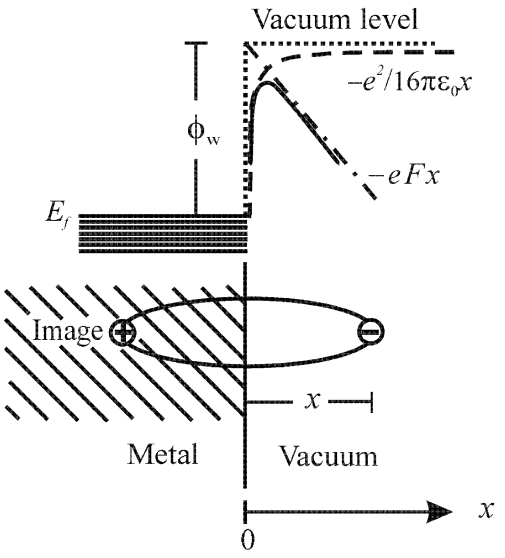

Fig. 1. Under the action of an applied electrical field F an electron tunnels from the metal with the work function ϕ_W into the vacuum, through the resultant surface barrier potential (solid line), which is obtained by superposing both the field potential (dash-dot line) and the image potential (dash line) on the surface barrier potential (dot line).

2. Theory

As shown in Fig. 1, under the action of an applied electrical field F an electron tunnels through the metal surface barrier potential into the vacuum, the metal surface in turn exerts an image force (attractive force) of magnitude $(1/4\pi\varepsilon_0)(e^2/4x^2)$ on the tunneling electron, where ε_0 is permittivity, x is the distance between the metal surface and the electron which is off the surface. Integrating the image force from ∞ to x, we have the image potential as fellows

$$u_i(x) = -e^2/16\pi\varepsilon_0 x \tag{1}$$

Note that Eq. (1) implies the potential energy of the electron at metal surface is equal to $-\infty$, so we assume that the image potential holds only for the values of x greater than some critical value x_0, approximately 1 Å, and that the image potential at $x=0$ coincides with the bottom energy of the barrier potential.

As shown in Fig. 2, for MIM tunnel junctions with a bias positive on the right-hand metal, a one-dimensional trapezoidal barrier potential model *without* the image force is

$$U_0(x) = \begin{cases} 0 & x<0 \\ \phi_1 + E_{fL} - (\phi_1 - \phi_2 + eV)\dfrac{x}{d}, & 0 \leqslant x \leqslant d \\ -eV & x>d \end{cases} \tag{2}$$

where d is the barrier width. For the tunneling electron in the insulator barrier region, there are the *two* image charges located, respectively, inside the two metal electrodes of the junction, each of which exert an attractive force (the image force) on the electron. The image potential, $U_i(x)$, inside the barrier region $(0<x<d)$ can be readily derived using mirror image method and is given by [4]

$$U_I(x) = \left(-\frac{e^2}{8\pi\varepsilon_0\varepsilon}\right)\left[\frac{1}{2x} + \sum_{n=1}^{\infty}\left(\frac{nd}{[(nd)^2 - x^2]} - \frac{1}{nd}\right)\right], \quad 0<x<d \tag{3}$$

If we let $d\to\infty$, Eq. (3) reduces to Eq. (1), which is simply the image potential from one metal surface (for vacuum $\varepsilon=1$). The $U_I(x)$ is awkward to handle, and a good approximation to Eq. (3) is given by [4]

$$U_i(x) \cong -1.15\lambda d^2/x(d-x), \quad 0<x<d \tag{4}$$

where $\lambda = (e^2 \ln 2)/8\pi\varepsilon_0\varepsilon d$ and ε is the dielectric constant of the barrier insulator layer. Note that the image potential $U_i(x)$ is in arbitrary shape and superposed on the trapezoidal barrier $U_0(x)$. Without and with the image force, the tunneling current through an effective trapezoidal barrier potential is given by [10]

$$j = \frac{4\pi m^* e}{h^3}\int_0^{\infty} dE_x D(E_x)\int_0^{\infty}[f(E) - f(E+eV)]dE_r \tag{5}$$

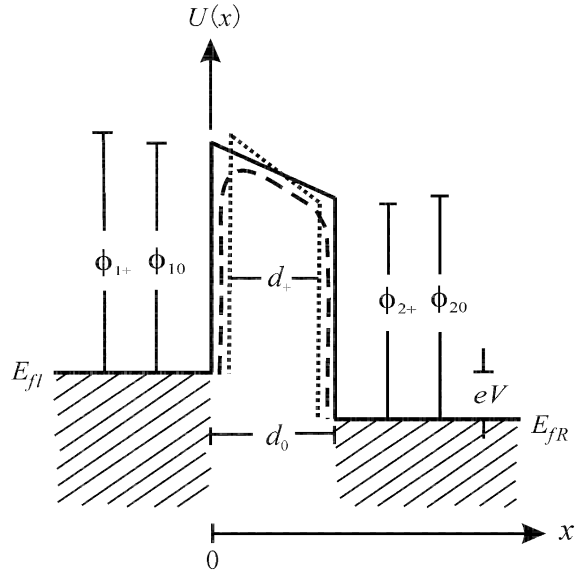

Fig. 2. One-dimensional actual *trapezoidal* barrier potential $U_0(x)$ (solid line) is used to model MIM tunnel junctions. As the image potential of *arbitrary* shape, $U_i(x)$, is superposed on the trapezoidal $U_0(x)$, there is to be a resultant barrier potential of *arbitrary* shape (dash line), to which a *trapezoidal* barrier $U_0(x)+U_i(x)$ (dot line) is equivalent. See text for detail.

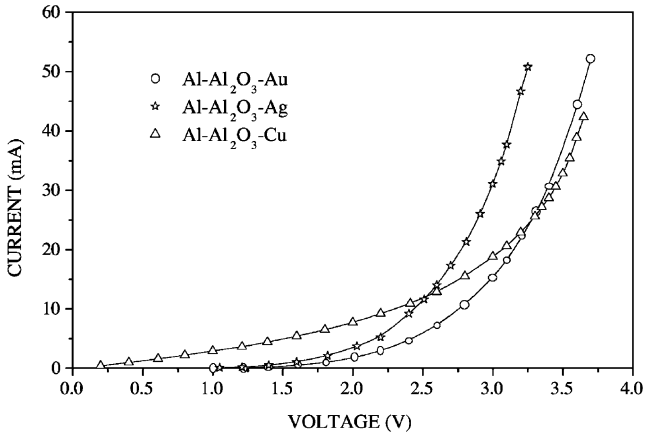

Fig. 3. The experimental I–V characteristics of the tunnel junctions at 77 K. Note that the lines serve as guides to the eye.

where $f(E)$ is the Fermi function, and E_x and E_r is the kinetic energy of the electron motion perpendicular and parallel to the junction interfaces, respectively. $D(E_x)$ is the tunneling probability. $D(E_x)$ without and with the $U_i(x)$ in WKB approximation is

$$D_0(E_x)=\exp\left\{-\frac{4\pi}{h}\int_{x_1(E_x)}^{x_2(E_x)}\sqrt{2m^*[U_0(x)-E_x]}\,dx\right\},\quad \text{without } U_i(x) \tag{6a}$$

and

$$D_i(E_x)=\exp\left\{-\frac{4\pi}{h}\int_{x_1(E_x)}^{x_2(E_x)}\sqrt{2m^*[U(x)_0+U_i(x)-E_x]}\,dx\right\},\quad \text{with } U_i(x) \tag{6b}$$

respectively, where x_1 and x_2 are the classical turning points, the potential $U_0(x)$ and $U_i(x)$ is given by Eqs. (2) and (4), respectively.

3. Experiment

The preparation of the junctions used to measure the experimental I–V curves was described in detail elsewhere [11]. At first, Al film strips were evaporated on glass slides, then the Al films were exposed to an oxygen glow discharge to grow a thin Al_2O_3 barrier layer on the Al film surface. This was followed by baking the samples in air at 200 °C for 30 min and then cooling the heated samples in air. Next MgF_2 film strips were evaporated over the edges of the oxidized Al film strips. Finally, the top metal electrode film strips of the Au (Ag, Cu) were deposited and the tunnel junctions of 2.5×2.5 mm^2 were obtained. The experimental I–V curve of the junctions were measured in a liquid nitrogen Dewar (77 K) and the top metal electrodes on the right were biased positively.

4. Results and discussion

The trapezoidal barrier parameters were determined by fitting the calculated I–V curves to the experimental I–V ones and the experimental I–V characteristics of the tunnel junctions with three different top electrodes are shown in Fig. 3. Note that as the bias voltage is less than 2.5 V, the tunneling current in the Cu-junction increases slower than that of the Au- and Ag-junction while the bias voltage increases, though the current through the Cu-junction is greater. Since the I–V characteristics of the tunnel junctions are linear at low voltage and become exponential at high voltage [4], the root-mean-square errors for the fitting, σ, which are shown in Table 1, is defined as

$$\sigma=\sum_{i=1}^{N}\left\{\frac{\left[\log(I_i^{(C)})-\log(I_i^{(E)})\right]^2}{N\left[\log(I_i^{(E)})\right]^2}\right\}^{1/2} \tag{7}$$

where $I_i^{(C)}$ and $I_i^{(E)}$ is the calculated and experimental current, respectively, and N is the number of the fitting points. The fittings were performed using a computer

Table 1
Three groups of the parameters: ϕ_{10}, ϕ_{20}, d_0; ϕ_{1-}, ϕ_{2-}, d_- and ϕ_{1+}, ϕ_{2+}, d_+ are for the *actual* barrier potential $U_0(x)$, $U_0(x)-U_i(x)$ and $U_0(x)+U_i(x)$, respectively, where $U_0(x)$ and $U_i(x)$ is the trapezoidal barrier potential and image potential, respectively. The root-mean-square errors, σ, are for I–V curve fitting. The effective mass of electrons, m^*, in Al_2O_3 was chosen to be 0.2 m_e, m_e is the free electron mass. See text for detail

	I–V curve fitting								Non I–V curve fitting		
Barrier models	$U_0(x)$				$U_0(x)+U_i(x)$				Extrapolation		
Actual barrier	$U_0(x)$				$U_0(x)-U_i(x)$				$U_0(x)+U_i(x)$		
Parameters	ϕ_{10} (eV)	ϕ_{20} (eV)	d_0 (Å)	σ	ϕ_{1-} (eV)	ϕ_{2-} (eV)	d_- (Å)	σ	ϕ_{1+} (eV)	ϕ_{2+} (eV)	d_+ (Å)
Al–Al_2O_3–Au	3.17	1.35	19.2	0.0248	3.01	1.45	20.8	0.0261	3.33	1.25	17.6
Al–Al_2O_3–Ag	3.22	0.93	23.3	0.0232	3.19	1.13	23.6	0.0233	3.25	0.73	23.0
Al–Al_2O_3–Cu	3.25	3.30	12.1	0.0213	3.21	3.67	12.0	0.0293	3.29	2.93	12.2

program in MATHEMETICA software and the data fits are shown in Fig. 4.

Three groups of the effective trapezoidal barrier parameters are given in Table 1. Of them, the first group of parameter ϕ_{10}, ϕ_{20}, d_0 were determined by fitting the calculated I–V curves, based on the barrier taken to be $U_0(x)$, to the experimental I–V curves (Eqs. (2) and (6a)). This is the routine case that without the image force the barrier parameters are determined by fitting the I–V curves. The second group of parameter ϕ_{1-}, ϕ_{2-}, d_- were determined by fitting the calculated I–V curves, based on the barrier taken to be $U_0(x)+U_i(x)$, to the experimental I–V curves (Eqs. (4) and (6b)). The reason why the notations for the second group of parameters have a suffix '−' is that the second group of parameters are for an actual barrier $U_0(x)-U_i(x)$, not for the $U_0(x)+U_i(x)$. To confirm this argument, the area A_- and A_0 of the two actual trapezoidal barrier, defined by the first and second group of the parameters, were calculated using the trapezoid area formula $A_0=(\phi_{10}+\phi_{20})d_0/2$ and $A_-=(\phi_{1-}+\phi_{2-})d_-/2$, respectively. It is found that A_- is *greater* than A_0, as seen in Table 2. It should be emphasized that the image potential $U_i(x)<0$ and the barrier parameters which were determined by fitting the I–V curves are only for the part of $U_0(x)$ in the resultant barrier potentials. Since the experimental I–V curves are independent of the theoretical barrier potential models and there is $A_->A_0$, the parameters ϕ_{1-}, ϕ_{2-}, d_- are characteristic of an effective trapezoidal barrier $U_0(x)-U_i(x)$, not $U_0(x)+U_i(x)$.

How to obtain the third group of the parameter ϕ_{1+}, ϕ_{2+}, d_+ for the actual barrier $U_0(x)+U_i(x)$? So far, the two groups of the barrier parameters, ϕ_{10}, ϕ_{20}, d_0 and ϕ_{1-}, ϕ_{2-}, d_- were determined by fitting the I–V curves and are characteristic of the actual effective trapezoidal barrier $U_0(x)$ and $U_0(x)-U_i(x)$, respectively. Thus, the third group of parameters, which is characteristic of an actual effective trapezoidal barrier $U_0(x)+U_i(x)$, was extrapolated and calculated using $\phi_{1+}=2\phi_{10}-\phi_{1-}$, $\phi_{2+}=2\phi_{20}-\phi_{2-}$, $d_+=2d_0-d_-$, as shown in Table 1. There are two ways to calculate the area of the effective trapezoidal barrier $U_0(x)+U_i(x)$: using $A_+=2A_0-A_-$ or $A_+=(\phi_{1+}+\phi_{2+})d_+/2$, but our calculation shows that there is no difference between the two ways. Similarly, there are other ways to calculate the width of the effective trapezoidal barrier for $U_0(x)+U_i(x)$: using $d_+=2A_+/(\phi_{1+}+\phi_{2+})$, but the two results for the width are not different from each other.

As shown in Table 1, for all the actual barriers the barrier height ϕ_{1i} ($i=0, -, +$) at the same Al–Al_2O_3 interface are just what they should be: they are approximately equal to each other. However, for Au-junction, due to the image force, the variations in the actual barrier heights at the Al–Al_2O_3 interface are that $\phi_{1+}-\phi_{10}=0.16$ eV and $\phi_{1+}-\phi_{1-}=0.32$ eV and at the Al_2O_3–Au interface are that $\phi_{2+}-\phi_{20}=-0.10$ eV and

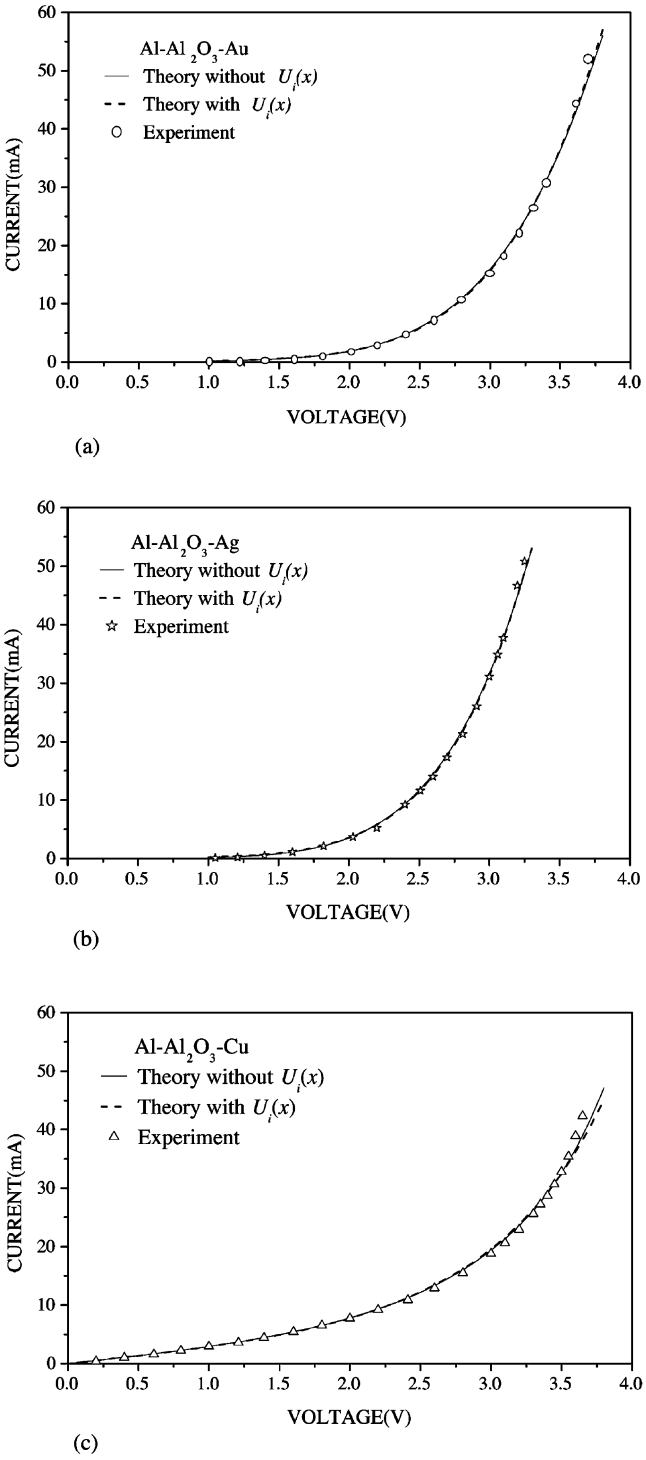

Fig. 4. The fitting of the theoretical I–V curves to the experimental ones for (a) the Au-, (b) Ag- and Cu-junction. The theoretical curves (solid lines and dash lines) were calculated based the trapezoidal barrier potential $U_0(x)$ and $U_0(x)+U_i(x)$, without and with the image potential $U_i(x)$, respectively. The root-mean-square errors, σ, for the fitting are shown in Table 1.

Table 2
The area A_0, A_- and A_+ is for the *actual* trapezoidal barrier potential $U_0(x)$, $U_0(x)-U_i(x)$ and $U_0(x)+U_i(x)$, respectively, where $U_0(x)$ and $U_i(x)$ is trapezoidal barrier potential and image potential, respectively. Note that the effect of the image force is to reduce the area of the barrier potential. See text for detail

	I–V curve fitting		Non *I–V* curve fitting	
Barrier models	$U_0(x)$	$U_0(x)+U_i(x)$	Extrapolation	
Actual barrier	$U_0(x)$	$U_0(x)-U_i(x)$	$U_0(x)+U_i(x)$	Area reduction
Area	A_0 (eV Å)	A_- (eV Å)	A_+ (eV Å)	$(A_+-A_0)/A_0$ (%)
Al–Al_2O_3–Au	43.39	46.38	40.40	−6.9
Al–Al_2O_3–Ag	48.35	50.98	45.72	−5.4
Al–Al_2O_3–Cu	39.63	41.28	37.98	−4.2

$\phi_{2+}-\phi_{2-}=-0.20$ eV Thus, as seen in Table 1, in contrast to Ag- and Cu-junction the variations in the barrier heights at the Al (bottom electrode)–Al_2O_3 interface of the Au-junction are *greater* than that at the Al_2O_3–Au (top electrode) interface.

On the other hand, the height ϕ_{2i} $(i=0, -, +)$ at the top electrode interfaces are quite different from each other. In particular, the ϕ_{2i} of the Cu-junction are much higher than that of the Au- and Ag-junction. Note that the barrier width d_i $(i=0, -, +)$ of the Cu-junction are much shorter than that of the Au- and Ag-junction. Nevertheless, as seen in Table 2, the *barrier area* for the Cu-junction is still smaller than that of the other junctions. The dependence of the ϕ_{2i} and d_i $(i=0, -, +)$ on the top metal electrodes can be understood as follows: at the interfaces oxygen atoms with dangling bonds can combine with Cu atoms but Au and Ag atoms, because Au is inactive and Ag is not attacked by oxygen under ordinary conditions but in presence of hydrogen sulfide, thus the copper oxide of one or two monolayer thickness was grown at the interface and an additional barrier must be considered. On the other hand, in comparison with the Au and Ag atoms, the Cu atoms with the smaller radius are easier to diffuse in to the Al_2O_3 barrier. The Auger depth profile measurements of the junctions have confirmed the above arguments [12]. Obviously, the oxidation and diffusion in the region of the interfaces not only result in the additional barrier layers, but also change the position definition of the metal mirrors of the electrodes, i.e. change the effects of the image force on the barrier parameters.

Since the effect of the image force is to reduce the area of the trapezoidal barrier potential $U_0(x)$ by rounding off the corner and reducing the width of the barrier, an equivalent effective trapezoidal barrier potential, which is used to model the deformed trapezoidal barrier with the rounded corner, in general, is not in proportion to the original one, $U_0(x)$. In other words, the trapezoidal barrier parameters for the actual $U_0(x)+U_i(x)$ are not in proportion to that for the actual $U_0(x)$. As seen in Table 1, for all the three types of junctions, the parameter ϕ_{1+} of the actual barrier $U_0(x)+U_i(x)$ is higher than the ϕ_{10} of the actual barrier $U_0(x)$. By contrast, for all the three types of junctions the ϕ_{2+} is lower than the ϕ_{20}, and for the Au- and Ag-junction but the Cu-junction the d_+ is shorter than the d_-. Nevertheless, as shown in Table 2, for all the three types of junctions the area of the actual barrier $U_0(x)+U_i(x)$ is *smaller* than that of the barrier with $U_0(x)$. These results just reflect the effect of the image force to reduce the barrier area.

As seen in Table 2, A_+ (the area of the actual barrier $U_0(x)+U_i(x)$) is smaller than A_0 (the area of the actual barrier $U_0(x)$), and for the Au-, Ag- and Cu-junction the area reduction is −6.9, −5.4 and −4.2%, respectively. Note that the image potential depends on the barrier width strongly and the image force has a greater influence on small barriers [4]. However, of the three junctions, the Cu-junction has not only the smallest barrier area, but also the smallest barrier area reduction. A qualitative explanation for this is that due to the diffusion and oxidation reaction of the Cu atoms in the interface region, the Al_2O_3–Cu interface becomes smeared and indistinct, and that for the Cu-junction the distance between the two actual metal mirrors of the Al and Cu electrodes is much longer than the barrier width shown in Table 1. As a result, though the effective actual barrier width of Cu-junction is smaller, the area reduction, i.e. the effect of the image force on the barrier potential is also smaller.

5. Summary

In most cases the effect of the image force on electron tunneling in MIM tunnel junctions has been neglected because this effect is thought to round off the barrier potential and make the barrier width slightly shorter. However, as the effective barrier parameters are to be determined, the difference between without and with the image force will become apparent and important. As the effective trapezoidal barrier parameters are determined by fitting theoretical *I–V* curves to the experimental ones, the parameters of the actual trapezoidal barrier $U_0(x)$, which is *not* with inclusion of the image potential

$U_i(x)$, are obtained if the theoretical I–V curves are calculated based on the barrier potential $U_0(x)$. In contrast, the parameters of the actual trapezoidal barrier $U_0(x)-U_i(x)$ are obtained if the theoretical I–V curves are calculated based on the barrier potential $U_0(x)+U_i(x)$. Thus, the parameters of the actual trapezoidal barrier $U_0(x)+U_i(x)$ can be obtained by extrapolating. The parameters (or the barrier shape) of the actual trapezoidal barrier $U_0(x)+U_i(x)$ are not in proportion to that of the trapezoidal barrier $U_0(x)$. The results show that for all the Au-, Ag- and Cu-junction the area of the actual trapezoidal barrier $U_0(x)+U_i(x)$ is smaller than that of the trapezoidal barrier $U_0(x)$, i.e. the effect of the image force is to reduce the barrier area. With inclusion of the image force, the variation in the effective barrier areas with the electrodes can be ascribed to the diffusion and oxidation reaction in the region of the junction interfaces, which results in smeared and indistinct interfaces and an increase in the actual distance between the two metal mirrors of the electrodes. Thus, due to the image force, the dependence of the effective barrier areas on the electrodes gives the information about the interfaces, in particular, about the metal mirrors of the electrodes in MIM tunnel junctions.

Acknowledgments

This work was supported by Research and Development Programs of Shenzhen.

References

[1] W. Sommerfeld, Z. Phyzik 47 (1928) 1.
[2] D. ter Haar, Problems in Quantum Mechanics, Pion Limited, London, 1975, p. 142.
[3] B. Roulet, M. Saint Jean, Am. J. Phys. 68 (2000) 319.
[4] (a) J.G. Simmons, J. Appl. Phys. 34 (1963) 1793
(b) J.G. Simmons, J. Appl. Phys. 34 (1963) 2581.
[5] W.F. Brinkman, R.C. Dynes, J.M. Rowell, J. Appl. Phys. 41 (1970) 1915.
[6] V.G. Valeyev, Phys. Low-Dimens. Struct. 5–6 (1999) 201.
[7] L. Mao, C. Tan, M. Xu, Microelectron. Reliab. 41 (2001) 927.
[8] J.S. Moodera, J. Nowak, R.J.M. van de Veerdonk, Phys. Rev. Lett. 80 (1998) 2941.
[9] J. Wang, S. Cardoso, P.P. Freitas, P. Wei, N.P. Barrasdas, J.C. Soares, J. Appl. Phys. 89 (2001) 6868.
[10] C.B. Duke, Theory of metal–barrier–metal tunneling, in: E. Burstein (Ed.), Tunneling Phenomena in Solids, Plenum, New York, 1969, p. 31.
[11] Q.Q. Shu, W.J. Wen, S.J. Xu, J. Appl. Phys. 65 (1989) 373.
[12] Q.Q. Shu, W.G. Ma, Appl. Phys. Lett. 61 (1992) 2524.